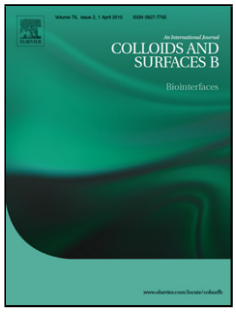

Title: NANOSTRUCTURED ELECTROCHEMICAL IMMUNOSENSOR FOR DETECTION OF SEROLOGICAL ALKALINE PHOSPHATASE

Authors: Estefani P. Simão, Isaac A.M. Frías, Cesar A.S. Andrade, Maria D.L. Oliveira

PII: S0927-7765(18)30504-6
DOI: https://doi.org/10.1016/j.colsurfb.2018.07.056
Reference: COLSUB 9512

To appear in: *Colloids and Surfaces B: Biointerfaces*

Received date: 13-3-2018
Revised date: 15-6-2018
Accepted date: 24-7-2018

Please cite this article as: Simão EP, Frías IAM, Andrade CAS, Oliveira MDL, NANOSTRUCTURED ELECTROCHEMICAL IMMUNOSENSOR FOR DETECTION OF SEROLOGICAL ALKALINE PHOSPHATASE, *Colloids and Surfaces B: Biointerfaces* (2018), https://doi.org/10.1016/j.colsurfb.2018.07.056

NANOSTRUCTURED ELECTROCHEMICAL IMMUNOSENSOR FOR DETECTION OF SEROLOGICAL ALKALINE PHOSPHATASE

Estefani P. Simão[1], Isaac A. M. Frías [2], Cesar A.S. Andrade[2,3], Maria D.L. Oliveira[1,2,3,*]

[1] Programa de Pós-Graduação em Ciências Biológicas, Universidade Federal de Pernambuco, 50670-901 Recife, PE, Brazil.

[2] Programa de Pós-Graduação em Inovação Terapêutica, Universidade Federal de Pernambuco, 50670-901 Recife, PE, Brasil

[3] Departamento de Bioquímica, Universidade Federal de Pernambuco, 50670-901 Recife, PE, Brazil.

*To whom correspondence should be addressed.

Maria D.L. Oliveira, Departamento de Bioquímica, UFPE, 50670-901, Recife, PE, Brazil. Phone: +55-81-2126.8450; Fax: +55-81-2126.8547

E-mail: m_danielly@yahoo.com.br

Graphical abstract

Graphical Abstract

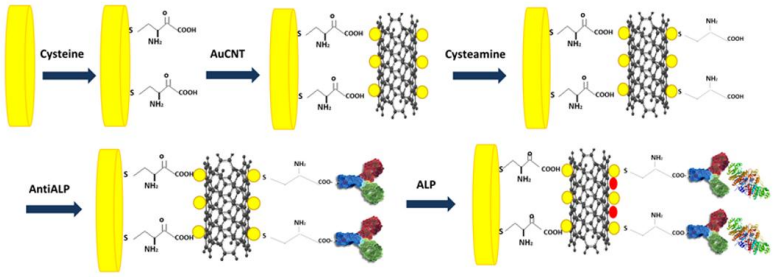

Highlights

- Alkaline phosphatase is an enzyme that plays an important role in calcification.
- A simple nanostructured platform was developed for ALP identification.
- Charge transfer resistance and cyclic voltammetry were effective parameters.
- The biosensor was capable of detecting a wide range of ALP concentrations.

Abstract

Alkaline phosphatase (ALP) is an enzyme that plays an important role in bone mineralization and skeletal growth. Variations in physiological levels of ALP have been correlated to diseases such as osteomalacia, Paget's disease and arterial calcifications. In this context, the integration of carbon nanotubes (CNT) within osteointegration implants has shown to increase ALP's mineralization activity in virtue of their surface chemistry and their morphological resemblance to collagen nanofibers. In this study we present the development and analytical application of an impedimetric immunosensor based in gold nanoparticle-decorated CNT, which characteristics are desirable in implantable biosensors. The device

effectively detects ALP within blood serum, a complex biological fluid where most expressed proteins can be found. Robustness and high sensitivity were attained by immobilizing covalently anti-ALP antibody as a specific probe towards ALP. Cyclic voltammetry, electrochemical impedance spectroscopy and atomic force microscopy were used to characterize the sensor system throughout mounting steps and real sample testing. Impedimetric responses were adjusted to a theoretical electrical circuit and charge transfer resistance showed to be an adequate parameter to evaluate the biorecognition process of the analyte. Additionally, amperometrical current variation and changes in topography found over the surface after positive samples evidenced biorecognition. The final biosensor showed excellent performance with two linear ranges from 0.5 to 50 $IU.L^{-1}$ and from 100 to 600 $IU.L^{-1}$; limits of detection were calculated as 0.25 and 84.6 $IU.L^{-1}$ respectively with a relative standard deviation lower than 5%. The device was found to be selective, avoiding protein c, a potential interferer occurring during inflammatory processes. The proposed strategy is promising for osteogenic applications where it can improve osteointegration implants by monitoring ALP activity.

Keywords: *Electrochemistry; immunosensor; alkaline phosphatase; carbon nanotubes; gold nanoparticles; nanotechnology.*

1. Introduction

Because of their rarity, most serological enzymes are subjects of clinical analysis regarding metabolic disorders and diseases [1]. Alkaline phosphatase (ALP) is a membrane-bound glycoprotein that promotes calcification at basic pH by reducing pyrophosphate levels [2]. ALP is considered a biomarker for colorectal cancer [3], sclerosing cholangitis [4], and its levels are monitored for predictive diagnosis of osteomalacia, Paget's disease, tumors, thyroid disorders, liver diseases, biliary obstructions and calcification processes in blood vessels of patients with heart disease [5]. Monitoring of ALP concentration is also relevant for treatment of chronical wounds since it plays an important role during bacterial biofilm formation [6].

Analytical detection of ALP is mostly performed through its catalytic activity and most methods are developed for classical platforms such as colorimetry [7], fluorometry [8], chromatography [9] and chemiluminescence [10]. Despite their high performance and reliability, their protocols are time-consuming, require trained personnel and specialized equipment. As an alternative, development of biosensing devices has grown rapidly and electrochemical methods stand out because of their fast response, simplicity and tendency towards miniaturization. Several nanomaterials are used as supporting transducers or tracers for sensitive electrochemical detection of ALP such as fluorescent carbon quantum dots, gold nanoparticles and metallic oxides [8, 11, 12], catalytic amplification with carbon nanotubes and DNAzyme nanowires [13, 14], and induced precipitation of metal oxides [15]. Indubitably, the association between nanostructures and biomolecules is of great interest in bionanotechnology and bioanalytical chemistry. In addition, previous studies have demonstrated that some nanostructures enhance the mineralization activity of ALP, especially multiwall carbon nanotubes [16]. However, as previously stated, these methodologies are unspecific and depend on the catalytic activity of the enzyme. Therefore, their response may be altered by cross-reactions and loss of activity due to improper reaction conditions.

Regardless of the usefulness of specific monitoring of ALP levels, immunosensing-based methods have been poorly exploited. Most reported immunosensors employ ALP-modified antibodies as secondary reporters for ELISA-based devices [17]. Therefore, in this work we propose a simple yet well-rounded strategy that employs a biocompatible electrochemical platform, for sensitive and specific detection of ALP in blood serum. The working principle of the biosensor rest on measuring the conductivity resulting from the physicochemical interaction between actual ALP and its specific antibody, which is covalently immobilized over gold-decorated multiwall carbon nanotubes. Initially, carbon nanotubes (CNT) were decorated with gold nanoparticles (*AuNPs)*, which were then conjugated with cysteamine (2-aminoethyl disulfide, AED). Finally, anti-alkaline phosphatase antibody (AntiALP) was covalently immobilized by EDC chemistry. As a result, we attained a sensitive label free biosensor to identify different levels of serological ALP. Because of the qualities of this platform, we proposed that this kind of device could be integrated on scaffolds for osteogenic applications where it can improve osteointegration implants by monitoring ALP activity, or in nanostructured healing dresses designed for chronical wounds.

2. Materials and methods

2.1 Materials

Alkaline phosphatase (ALP), anti-alkaline phosphatase antibody (AntiALP), multiwall carbon nanotubes (CNT), potassium ferrocyanide, potassium ferricyanide, bovine serum albumin (BSA), cysteine, cysteamine, 1-ethyl-3-(3-dimethylaminopropyl) carbodiimide (EDC), N-hydroxysuccinimide (NHS) were purchased from Sigma Chemical (St. Louis, MO, USA). Blood serum samples were obtained from Laboratório Central do Estado de Pernambuco

(LACEN). All chemicals and analytical grade solvents were used as received without further purification.

2.2 Synthesis of AuNPs and AuCNT

Murphy's method [18] was followed with slight modifications. Briefly, trisodium citrate (0.5 mL) was mixed with 0.01 M $HAuCl_4 \bullet 3H_2O$ (1:1) and the solution was completed with deionized water (v = 18 mL) under cooling. Thereafter, 0.1 M $NaBH_4$ was added under stirring until a pink colored solution was obtained indicating that AuNPs were formed.

AuCNT system was obtained by quickly mixing 9.3 mg of CNT with 10 mL of AuNPs solution previously obtained, favoring electrostatic interaction between CNT and AuNPs. Thereafter, 6 mL of ethanol were added to the previous mixture under vigorous stirring for 10 h. The addition of ethanol reduces the surface tension between the CNT and the water resulting in physical adsorption of the AuNPs to the CNT [19]. AuCNT were washed five times by centrifugation at 10,000 x g and finally dried at 70°C.

2.3 Preparation of the immunosensor

A gold electrode (2 mm diameter) was polished with 0.05 µm alumina paste, rinsed with deionized water and dried at room temperature. Subsequently, 5µL of a 70 mM cysteine solution were dropped over the electrode surface and set to incubation for 10 min. Following, 5µL of the AuCNT solution were chemisorbed by gold-thiol interaction over the Cys-modified electrode and set to incubation for 30 min. Thereafter, 5µL of a 70mM of AED were conjugated to AuNPs by chemical adsorption. This step was important to provide a carboxyl chemical group for adequate immobilization of the antibody. To activate the carboxyl residues, 5µL of an acetate buffer solution (pH 5.0) containing a mixture of 2mM 1-ethyl-3-(3-dimethylaminopropyl) carbodiimide (EDC) and 5mM N-hydroxysuccinimide (NHS) (1:1, v/v)

were added and set to incubation. Passed 2 h, 5μL of a 225 $\mu g.mL^{-1}$ AntiALP solution were dropped, and set to incubation for 10 min of to promote covalent binding. Finally, bovine serum albumin (BSA) was used to block non-specific binding sites. The construction of the platform Cys-AuCNT-AntiALP-modified working electrode-probe-BSA sensor is schematized in Fig. 1.

2.4 Electrochemical measurements

All electrochemical measurements were performed in triplicate on a PGSTAT 128N potentiostat/galvanostat (Metrohm Autolab Inc., Netherlands). The experiments were carried out using a three-electrode array with a platinum wire counter electrode, an Ag/AgCl reference electrode saturated with a KCl solution, and the AuCNT-AntiALP-modified sensor. All measurements were performed in the presence of 10mM $K_4[Fe(CN)_6]^{4-}/K_3[Fe(CN)_6]^{3-}$ redox pair (1:1, v/v). Electrochemical impedance spectroscopy (EIS) response was analyzed in a frequency range between 100 mHz and 100 kHz with an applied potential of 10 mV. Cyclic voltammetry was performed in a potential range between -0.2 and +0.7 V at $50mV.s^{-1}$ scan rate.

2.5 Evaluation of Bioactivity and, sensitivity and specificity analysis

All measurements were performed in triplicate, using 5 μL volume samples dropped over the immunosensor surface and let to incubate for 15 min before reading the electrochemical response. Sensitivity was evaluated by studying aqueous ALP standard solutions and dilutions from ALP-spiked human umbilical cord blood serum samples at different ALP concentrations (0.5, 1, 5, 10, 50, 100, 200, 300, 400, 500 and 600 $IU.L^{-1}$). The concentration of ALP of all samples was previously measured through a spectrophotometric method. To test specificity, the immunosensor was exposed to an aqueous solution containing 10 $mg.mL^{-1}$ C-reactive protein (CRP), a serological marker found to be quite elevated in

patients suffering from cardiovascular diseases, tumors, rheumatic diseases and bacterial infections.

2.6 Topographical analysis

AFM analysis were performed using a SPM-9700 atomic force microscope (Shimadzu, Tokyo, Japan) in noncontact mode at room temperature. Aluminum-coated silicon cantilevers (Multi 75AL, NCHR, resonant frequency = 75 kHz, force constant = 3 $N.m^{-1}$) were used. The images (512 points per line) were collected with a scan rate of 1.0 Hz in a scan area of 5.0 × 5.0 µm. Furthermore, images were collected and analyzed using AFM Gwyddion software [20].

3. Results and discussion

3.1 Topographical characterization

3D AFM images of the modified electrode are shown in Fig. 2. Atomic force microscopy was used to evaluate the modification process of the gold electrode and investigate the changes of the immunosensor before and after antibody-antigen complex formation. Pristine gold surface (Fig. 2a) was exposed to cysteine and chemisorption occurs immediately after contact, introducing functionality to the surface. The self-assembled monolayer presents a maximum height of 37 nm (Fig. 2b) and the change from smooth surface morphology after the adsorption of the Cys molecules was found similar to previous published reports [21]. The subsequent immobilization of the AuCNT-AED system (Fig. 2c) results in an increase in height (63 nm) and surface rugosity due to the presence of dispersed nanostructures. Once anti-ALP and BSA were conjugated in the biosensor (Fig. 2d), an increase in height to 75 nm was observed. The difference in height (12 nm) from the previous step is similar to that reported in previous works [22, 23], and is assigned to the typical height of the antibody layer. Following (Fig. 2e), the immunosensor was exposed to an ALP positive sample. One observes a drastic change in height

and topography after the specific interaction with ALP resulted in coverage of the sensor surface, indicating that the ALP was successfully recognized. For the most likely, the resultant morphology occurs as a result of the nonlinear relation between binding sites and ligand's concentration, as we will discuss in the following sections. In contrast (Fig. 2f), when the C-protein interferer sample is tested, there were no significant changes on the sensor surface, thus confirming that, even after being adsorbed on the surface of the gold-decorated CNT, AntiALP retained its antigen recognition capability, suggesting high selectivity of this sensing platform.

3.2 Electrochemical characterization

Fig. 3a shows the cyclic voltammograms of the immunosensor assembly process. Pristine gold electrode presents well-defined peak currents demonstrating a typical reversible electrolytic reaction of the redox probe. Cysteine chemisorption is evidenced in the repulsion effect of the potassium ferro-ferricyanide towards the negative characteristic of the cysteine [24]. AuCNTs were then immobilized to the Cys layer, causing a new decrease in the peak currents and a blockage of the electron transfer. In addition, after adsorption of AED an increase in the amperometric currents due to the positive charge of this molecule was verified. The adsorption causes the attraction of the redox probe that is negatively charged at pH 7.4. Furthermore, EDC: NHS activated the AED carboxyl groups favoring the covalent binding with the amine groups present in the AntiALP, causing a decrease in the electron transfer resistance of the system. BSA was added to the sensor system to block unspecific interactions, the addition of this protein caused a reduction in the voltammogram peak currents.

In Fig. 3b, Nyquist impedance data revealed a semicircle response. Analytical examination of the obtained EIS data was performed through the equivalent circuit shown in the inset of Fig. 3b. This circuit allows to evaluate the recognition capability of the immunosensor through theoretical calculations modeled using NOVA 1.11 software (Metrohm

Autolab Inc., Netherlands). This spectrum corresponds to an electron transfer limited process and from its diameter the electron transfer resistance (Rct) can be inferred. For instance, EIS analysis of the gold electrode showed a lower charge transfer resistance (Rct = 0.57 kΩ ± 0.04) compared with subsequent steps (Table 1). Chemisorption of Cys monolayer obstructed the motility of the electrochemical probe and therefore contributed to the increase in the semicircle diameter (Rct = 4.40 kΩ ± 0.25). Similarly, immobilization of AuNpCNT resulted in an increase in the Rct (10.2 kΩ ± 0.14) evidencing further blockage of the electron transfer. Despite the semiconducting properties of CNT, defects found over the surface of multi-walled CNT are associated to an insulating nature [25]. After the addition of AED, the attraction between the positive charge of amino group in AED and negative charge of $[Fe(CN)_6]^{3-/4-}$, leads to the accumulation of $[Fe(CN)_6]^{3-/4-}$ on the electrode interface causing a dramatic decrease in the impedimetric response (Rct = 0.23 kΩ ± 0.01). After modification with AuCNT-AntiALP system, EIS response shows a higher interfacial charge transfer resistance (Rct = 3.77 kΩ ± 0.43). The Rct increased again after BSA adsorption, indicating the formation of the sensor layer due to the hindering of the electron transfer (Rct = 4.83 kΩ ± 0.71).

3.2 Electrochemical detection of ALP

Reproducibility and standard experimental deviation (S.D.) were assessed as the result of three replicates performed for each sample. EIS spectra resulting from the bio-detection are presented in Fig. 4. A gradual increment in the semicircle diameter was found in both standard solutions (Fig. 4a) and spiked serum samples (Fig. 4b). In concordance with the AFM results, this behavior is correlated with the formation of an immunocomplex resulting from the binding of the antibody to the specific antigen that results in additional blockage for the passage of the redox probe ions [26]. We found that Rct was a convenient component to evaluate the antigen-antibody interaction in terms of their relative variation as defined by:

$$\Delta Rct\% = \frac{Rct(immunosensor+ALP)-Rct(immunosensor)}{Rct(immunosensor)} x100 \qquad \text{(Eq.1)}$$

where $R_{ct(immunosensor+ALP)}$ is the value of the charge transfer resistance for recognition of the ALP, and $R_{ct(immunosensor)}$ corresponds to the resistance value of charge transfer of the sensor before the interaction with ALP. All resultant values are shown in Table 1. The relation between ΔRct% and ALP concentration reflects the performance of the immunosensor.

Calibration curves are shown in Fig. 5, two linear ranges could be found. From aqueous ALP solutions (Fig. 5a), the first one was from the 0.5 to 50 $IU.L^{-1}$ range with a logarithmic regression equation of ΔRct% = 31.23+23.71 *log* [ALP] (R^2 = 0.96). The limit of detection (LOD) estimated at a s/n of 3.3σ (where σ is the standard deviation of a blank sample, n=3) was 0.25 $IU.L^{-1}$, and limit of quantification (LOQ) estimated at a s/n of 10 σ was 0.76 $IU.L^{-1}$. The other calibration range from 100 to 600 $IU.L^{-1}$ with a linear regression equation of ΔRct% = 0.31+124.27 [ALP] (R^2 = 0.98) resulted in a LOD = 84.6 $IU.L^{-1}$ and a LOQ = 256.4 $IU.L^{-1}$. In a like manner to aqueous solutions, the calibration curve obtained from the spiked serum samples (Fig. 5b) also showed two linear ranges with the only difference that maximum concentration of detection was 500 $IU.L^{-1}$. From 0.5 to 50 $IU.L^{-1}$ range, the logarithmic regression equation was ΔRct% = 215.84+103.11 *log* [ALP] (R^2 = 0.96) with a LOD = 0.15 $IU.L^{-1}$ and a LOQ = 0.45 $IU.L^{-1}$. Correspondingly, the second range from 100 to 500 $IU.L^{-1}$ was adjusted to a linear regression equation of ΔRct% = 1.41+556.25 [ALP] (R^2 = 0.95) resulted in a LOD = 133.1 $IU.L^{-1}$ and a LOQ = 403.3 $IU.L^{-1}$. ALP serological levels in healthy adults usually vary between 20-140 $IU.L^{-1}$ [27], therefore the proposed immunosensor is promising for reliable ALP monitoring with a sensitivity much lower than many previous reports (Table 2).

Taking into consideration the change in topography of the immunosensor surface after ALP biorecognition and the concentration-dependent double linearity, it was confirmed that immunosensing of ALP is strongly affected by cooperative binding effects. This behavior

occurred in both aqueous standard samples and serum spiked samples and is associated to the non-linear relationship between the number of binding sites of the antibody and ALP's concentration. Additionally, in both samples the further increase of ALP concentration resulted in a gradual Rct saturation. The affinity of the ligands towards specific binding sites such as antibodies, depend on the amount of ligand bound [28]. A similar behavior has been observed before in other electrochemical biosensors [29, 30]. Moreover, surface coating (θ) was calculated as follows [31]:

$$\theta = 1 - \left(\frac{Rct(sensor\ system)}{Rct(ALP)}\right) \qquad \text{(Eq.2)}$$

The degree of surface coating is based on the ratio between Rct of the sensor before and after ALP detection at different concentrations. The surface coating is directly proportional to the increase in the ALP concentration. Θ plot as a function of ALP is shown in Fig. 6. Of note, the value of Θ increases with increasing ALP concentration. Surface coating at 600 $IU.L^{-1}$ was found to be 75% for synthetic samples (Fig. 6a) and 95% for serum-spiked samples (Fig. 6b).

3.3 Immunosensor selectivity

The selectivity of the immunosensor was evaluated using a 10 $mg.mL^{-1}$ C-reactive protein (CRP) and glucose mix (1:1 v/v). CRP is a molecular reporter commonly found during inflammatory processes that presents synergistic action towards serological ALP [32]. No significant response was obtained in terms of Rct ($6.23\ k\Omega \pm 0.18$) nor topography change after exposure to the mix. Confirming as previously mentioned that the bio-interaction process occurs from the attraction between specific antigen and antibody guided by physicochemical interactions, which, despite being weak bonds, reflect the specificity of immunoreaction [33].

4. Conclusions

We developed a simple nanostructured platform that simultaneously presents desirable characteristics for osteointegration implants and alkaline phosphatase biosensing applications. Covalent immobilizations were preferred throughout the construction of the platform resulting in a robust non-leaching immunosensor. AntiALP retained its biological activity after immobilization. The proposed device is able to detect APL from 0.5 to 500 $IU.L^{-1}$ with very low limits of detection and quantification. Compared to other ALP sensors, the present work excels in simplicity since pre-analytical preparations are not required and moreover, it presents an extensive linear range for quantification. The time for diagnosis (after the platform is constructed) takes only 15 min. These results are an important basis for the development of sensitive ALP sensor and a useful strategy for diagnosis of several diseases and also bacterial growth.

Acknowledgements

The authors are grateful for the support of the Brazilian National Council for Scientific and Technological Development/CNPq (grant 302885/2015-3 and 302930/2015-9), MCT/FINEP, PROPESQ/UFPE. Pontes would like to thank Capes for MSc scholarship. Isaac A. M. Frias would like to thank CAPES and FACEPE for postdoctoral fellowships.

References

1. Huggett, R.J., *Biomarkers: biochemical, physiological, and histological markers of anthropogenic stress*. 2018: CRC Press.
2. Sharma, U., D. Pal, and R. Prasad, *Alkaline Phosphatase: An Overview.* Indian Journal of Clinical Biochemistry, 2014. **29**(3): p. 269-278.
3. Hung, H.-Y., et al., *Preoperative alkaline phosphatase elevation was associated with poor survival in colorectal cancer patients.* International Journal of Colorectal Disease, 2017. **32**(12): p. 1775-1778.

4. de Vries, E.M., et al., *Alkaline phosphatase at diagnosis of primary sclerosing cholangitis and 1 year later: evaluation of prognostic value.* Liver International, 2016. **36**(12): p. 1867-1875.
5. Styne, D.M., *Disorders of Calcium Metabolism and Bone*, in *Pediatric Endocrinology: A Clinical Handbook*. 2016, Springer International Publishing: Cham. p. 123-157.
6. Danikowski, K.M. and T. Cheng, *Alkaline Phosphatase Activity of Staphylococcus aureus Grown in Biofilm and Suspension Cultures.* Current Microbiology, 2018.
7. Hu, Q., et al., *Sensitive and selective colorimetric assay of alkaline phosphatase activity with Cu(II)-phenanthroline complex.* Talanta, 2017. **163**: p. 146-152.
8. Xu, A.-Z., et al., *Fluorometric determination of the activity of alkaline phosphatase based on the competitive binding of gold nanoparticles and pyrophosphate to CePO4:Tb nanorods.* Microchimica Acta, 2018. **185**(6): p. 288.
9. Lakra, S., V.J. Jadhav, and S.R. Garg, *Development of a Chromatographic Method for the Determination of Alkaline Phosphatase Activity in Pasteurized Milk.* Food Analytical Methods, 2016. **9**(7): p. 2002-2009.
10. Mei, Y., et al., *Fluorescence quenching based alkaline phosphatase activity detection.* Talanta, 2018. **176**: p. 52-58.
11. Niu, F., et al., *Electrochemically generated green-fluorescent N-doped carbon quantum dots for facile monitoring alkaline phosphatase activity based on the Fe3+-mediating ON-OFF-ON-OFF fluorescence principle.* Carbon, 2018. **127**: p. 340-348.
12. Qu, F., et al., *Novel turn-on fluorescent detection of alkaline phosphatase based on green synthesized carbon dots and MnO2 nanosheets.* Talanta, 2017. **165**: p. 136-142.
13. Zhao, L., et al., *Gold Nanoparticle-Decorated Single-Walled Carbon Nanotubes as a Catalytic Amplification Platform for the Electrochemical Detection of Alkaline Phosphatase Activity.* Internacional Journal of Eletrochemical Science, 2018. **13**(2): p. 1293-1307.
14. Liu, Y., et al., *Sensitive electrochemical assay of alkaline phosphatase activity based on TdT-mediated hemin/G-quadruplex DNAzyme nanowires for signal amplification.* Biosensors and Bioelectronics, 2017. **87**: p. 970-975.
15. Shen, C., et al., *A single electrochemical biosensor for detecting the activity and inhibition of both protein kinase and alkaline phosphatase based on phosphate ions induced deposition of redox precipitates.* Biosensors and Bioelectronics, 2016. **85**: p. 220-225.
16. Zancanela, D.C., et al., *Defective multilayer carbon nanotubes increase alkaline phosphatase activity and bone-like nodules in osteoblast cultures.* Journal of nanoscience and nanotechnology, 2016. **16**(2): p. 1437-1444.
17. Lim, S.A. and M.U. Ahmed, *Electrochemical immunosensors and their recent nanomaterial-based signal amplification strategies: a review.* RSC Advances, 2016. **6**(30): p. 24995-25014.
18. Jana, N.R., L. Gearheart, and C.J. Murphy, *Seeding Growth for Size Control of 5–40 nm Diameter Gold Nanoparticles.* Langmuir, 2001. **17**(22): p. 6782-6786.
19. Shi, Y., R. Yang, and P.K. Yuet, *Easy decoration of carbon nanotubes with well dispersed gold nanoparticles and the use of the material as an electrocatalyst.* Carbon, 2009. **47**(4): p. 1146-1151.
20. Nečas, D. and P. Klapetek, *Gwyddion: an open-source software for SPM data analysis.* Open Physics, 2012. **10**(1): p. 181-188.
21. Hashemi, P., et al., *Fabrication of a novel impedimetric sensor based on L-cysteine/Cu (II) modified gold electrode for sensitive determination of ampyra.* Analytica chimica acta, 2017. **984**: p. 185-192.
22. Simão, E.P., et al., *Biosensor Based on Cysteine Monolayer and Monoclonal Antibody for Specific Detection of Aflatoxin B1in Rice.* Journal of the Brazilian Chemical Society, 2015.
23. Hao, C., et al., *A self-assembled monolayer based electrochemical immunosensor for detection of leukemia K562A cells.* Electrochemistry Communications, 2007. **9**(6): p. 1359-1364.
24. Yang, L. and Y. Li, *AFM and impedance spectroscopy characterization of the immobilization of antibodies on indium–tin oxide electrode through self-assembled monolayer of epoxysilane*

and their capture of Escherichia coli O157:H7. Biosensors and Bioelectronics, 2005. **20**(7): p. 1407-1416.
25. Dresselhaus, M.S., et al., *Carbon nanotubes*, in *The Physics of Fullerene-Based and Fullerene-Related Materials*. 2000, Springer. p. 331-379.
26. Serafín, V., et al., *Determination of prolactin hormone in serum and urine using an electrochemical immunosensor based on poly(pyrrolepropionic acid)/carbon nanotubes hybrid modified electrodes.* Sensors and Actuators B: Chemical, 2014. **195**: p. 494-499.
27. Acharya, S., et al., *Serum alkaline phosphatase in oral squamous cell carcinoma and its association with clinicopathological characteristics.* South Asian Journal of Cancer, 2017. **6**(3): p. 125-128.
28. Stefan, M.I. and N. Le Novère, *Cooperative binding.* PLoS computational biology, 2013. **9**(6): p. e1003106.
29. Hatamluyi, B. and Z. Es' haghi, *A layer-by-layer sensing architecture based on dendrimer and ionic liquid supported reduced graphene oxide for simultaneous hollow-fiber solid phase microextraction and electrochemical determination of anti-cancer drug imatinib in biological samples.* Journal of Electroanalytical Chemistry, 2017. **801**: p. 439-449.
30. Hajian, R., Z. Tayebi, and N. Shams, *Fabrication of an electrochemical sensor for determination of doxorubicin in human plasma and its interaction with DNA.* Journal of pharmaceutical analysis, 2017. **7**(1): p. 27-33.
31. Avelino, K.Y., et al., *Attomolar electrochemical detection of the BCR/ABL fusion gene based on an amplifying self-signal metal nanoparticle-conducting polymer hybrid composite.* Colloids and Surfaces B: Biointerfaces, 2016. **148**: p. 576-584.
32. Karakaya, C., et al., *Serum IL-6 and CRP levels in patients with trauma involving low-extremity bone fractures.* Eastern Journal of Medicine, 2013. **18**(4): p. 176.
33. Seenivasan, R., et al., *An electrochemical immunosensing method for detecting melanoma cells.* Biosensors and Bioelectronics, 2015. **68**: p. 508-515.

Figure Captions

Figure 1. Schematic representation of the biosensor assembly steps.

Figure 2. 3D AFM images showing immunosensor assembly steps: a) gold surface, b) cysteine monolayer, c) cysteine-AuCNT-AED, d) cysteine-AuCNT-AED-AntiALP, e) sensor system-ALP, f) sensor system-negative control.

Figure 3. Cyclic Voltammogram **(a)** and Nyquist plots **(b)** of each step of the immunosensor assembly: (a)Au; (b)Au-Cys; (c)Au-Cys-AuCNT; (d)Au-Cys- AuCNT-AED;(e) Au-Cys-

AuCNT-AED-EDC:NHS; (f)Au-Cys-AuCNT-AED-EDC:NHS-AntiALP; (g) Au-Cys-AuCNT-AED-EDC:NHS-AntiALP-BSA.

Figure 4. Nyquist plot of the Faradaic impedance measurements of the biosensor for interaction with synthetic (a) and serological ALP (b): (a) Sensor system; (b) 0.5 $IU.L^{-1}$; (c) 1 $IU.L^{-1}$; (d) 5 $IU.L^{-1}$; (e) 10 $IU.L^{-1}$; (f) 50 $IU.L^{-1}$; (g)100 $IU.L^{-1}$; (h) 200 $IU.L^{-1}$; (i) 300 $IU.L^{-1}$; (j) 400 $IU.L^{-1}$; (k) 500 $IU.L^{-1}$; (l) 600 $IU.L^{-1}$.

Figure 5. Relative charge transfer ($\Delta R_{ct}\%$) of the immunosensor for synthetic **(a)** and serological ALP **(b)** at different concentrations (0.5-600 $IU.L^{-1}$).

Figure 6. Surface coating (θ) of the immunosensor for synthetic **(a)** and serological ALP **(b)** at different concentrations.

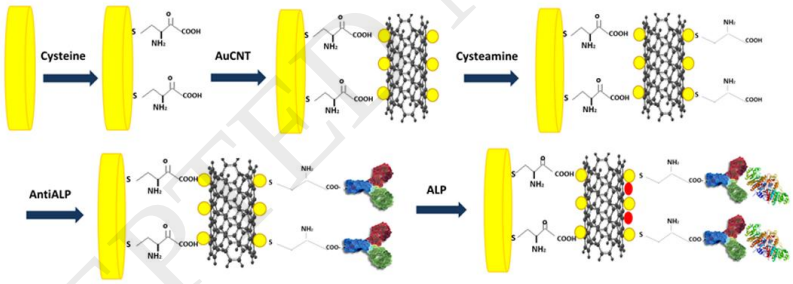

Fig. 1

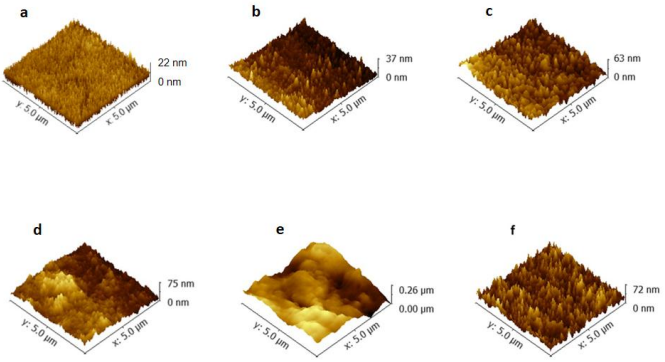

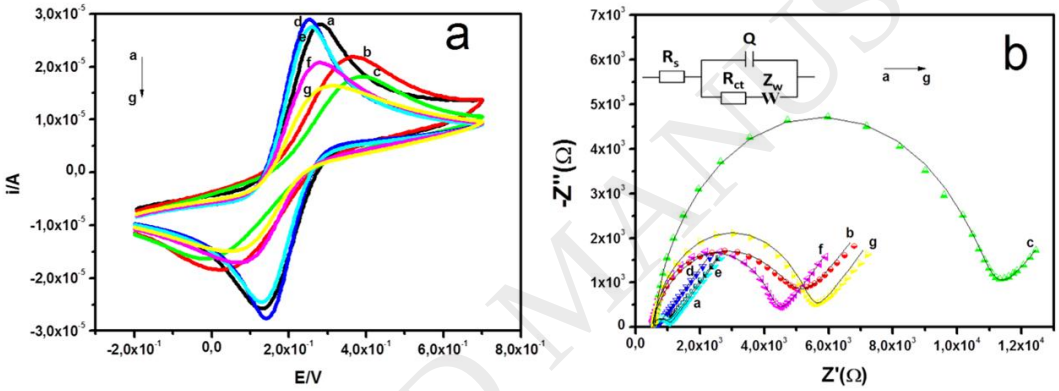

Fig. 3

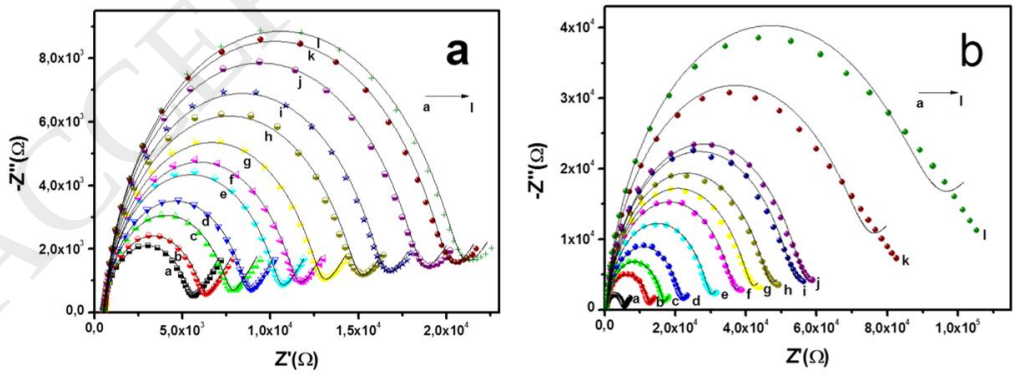

Fig. 4

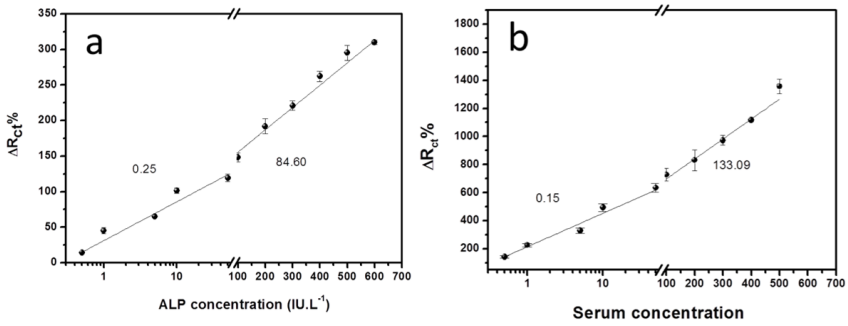

Fig. 5

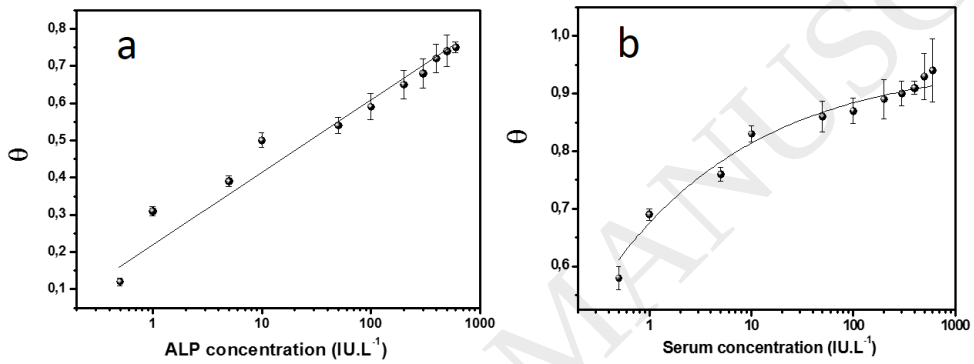

Fig. 6

Table Captions

Table 1. The equivalent circuit parameters of the immunosensor before and after ALP interaction.

Table 1

Modified electrode	**R_{ct} (kΩ)**	**Q^{a*} (μF)**	**n^{b*}**
Au	0.57±0.04	11.3	0.647
Cysteine (Cys)	4.40±0.25	3.08	0.822
Cys – AuCNT	10.2±0.14	9.32	0.941
Cys- AuCNT- cysteamine	0.23±0.18	4.78	0.397
Cys - AuCNT- cysteamine -AntiALP	3.77±0.43	7.46	0.912
Cys - AuCNT- cysteamine-AntiALP-BSA	4.83±0.71	6.53	0.908
Biosystem-ALP [0.5 $IU.L^{-1}$]	5.52±0.08	6.35	0.911
Biosystem-ALP [1 $IU.L^{-1}$]	7.00±0.19	6.29	0.914
Biosystem-ALP [5 $IU.L^{-1}$]	7.98±0.08	6.10	0.917
Biosystem-ALP [10 $IU.L^{-1}$]	9.72±0.48	6.16	0.928
Biosystem-ALP [50 $IU.L^{-1}$]	10.60±0.26	6.31	0.926
Biosystem-ALP [100 $IU.L^{-1}$]	12.00±0.30	6.27	0.926
Biosystem-ALP [200 $IU.L^{-1}$]	14.10±0.50	6.62	0.916
Biosystem-ALP [300 $IU.L^{-1}$]	15.55±0.30	6.25	0.926
Biosystem-ALP [400 $IU.L^{-1}$]	17.50±0.35	6.05	0.931
Biosystem-ALP [500 $IU.L^{-1}$]	19.10±0.51	6.04	0.931
Biosystem-ALP [600 $IU.L^{-1}$]	19.80±0.15	6.06	0.930
Biosystem-Serum [0.5 $IU.L^{-1}$]	11.70±0.45	6.02	0.901
Biosystem-Serum [1 $IU.L^{-1}$]	15.80±0.55	5.61	0.909
Biosystem-Serum [5 $IU.L^{-1}$]	20.80±0.95	5.71	0.906
Biosystem-Serum [10 $IU.L^{-1}$]	28.70±0.72	5.88	0.9
Biosystem-Serum [50 $IU.L^{-1}$]	35.50±0.36	5.60	0.906
Biosystem-Serum [100 $IU.L^{-1}$]	40.00±0.92	5.57	0.905
Biosystem-Serum [200 $IU.L^{-1}$]	45.00±0.50	5.55	0.905
Biosystem-Serum [300 $IU.L^{-1}$]	51.80±0.90	5.37	0.908
Biosystem-Serum [400 $IU.L^{-1}$]	58.80±0.70	5.54	0.904
Biosystem-Serum [500 $IU.L^{-1}$]	70.40±0.90	5.68	0.927
Biosystem-Serum [600 $IU.L^{-1}$]	88.50±0.76	5.90	0.926
Biosystem-Negative control	5.58±0.18	5.78	0.813

[a*]Constant-phase element; [b*]Indicates dispersion of relaxation time due to lack of surface homogeneity.

Table 2. Analytical comparison of the biosensors for quantification of ALP.

Table 2

Technique	**Transducer**	**Range of Detection**	**References**
Eletrochemical	Indium tin oxide (ITO) film on glass and p-nitrophenyl phosphate	5-180 UI/L	[3]
Fluorimetric	8-Quinolyl phosphate	1.0–16.0 UI/L	[4]
Colorimetric	Conjugated gold nanoparticle/adenosine triphosphate		[2]
Eletrochemical	$MgCl_2$ and phenyl Phosphate	0-300UI/L	[14]
Eletrochemical	SAM of cisteine and AuCNT modified bound to an antibody	0.5-600 UI/L	Present work